Catalysts **2015**, *5*, 58-76; doi:10.3390/catal5010058

OPEN ACCESS

catalysts

ISSN 2073-4344

www.mdpi.com/journal/catalysts

Article

Effect of Ce and Zr Addition to Ni/SiO_2 Catalysts for Hydrogen Production through Ethanol Steam Reforming

Jose Antonio Calles *, Alicia Carrero, Arturo Javier Vizcaíno and Montaña Lindo

Department of Chemical and Energy Technology, Rey Juan Carlos Universtity, c/Tulipán, s/n, Móstoles 28933, Spain; E-Mails: alicia.carrero@urjc.es (A.C.); arturo.vizcaino@urjc.es (A.J.V.); puinaction@yahoo.es (M.L.)

* Author to whom correspondence should be addressed; E-Mail: joseantonio.calles@urjc.es; Tel.: +34-91-488-7378; Fax: +34-91-488-7068.

Academic Editors: Morris D. Argyle and Calvin H. Bartholomew

Received: 31 October 2014 / Accepted: 7 January 2015 / Published: 30 January 2015

Abstract: A series of Ni/$Ce_xZr_{1-x}O_2$/SiO_2 catalysts with different Zr/Ce mass ratios were prepared by incipient wetness impregnation. Ni/SiO_2, Ni/CeO_2 and Ni/ZrO_2 were also prepared as reference materials to compare. Catalysts' performances were tested in ethanol steam reforming for hydrogen production and characterized by XRD, H_2-temperature programmed reduction (TPR), NH_3-temperature programmed desorption (TPD), TEM, ICP-AES and N_2-sorption measurements. The Ni/SiO_2 catalyst led to a higher hydrogen selectivity than Ni/CeO_2 and Ni/ZrO_2, but it could not maintain complete ethanol conversion due to deactivation. The incorporation of Ce or Zr prior to Ni on the silica support resulted in catalysts with better performance for steam reforming, keeping complete ethanol conversion over time. When both Zr and Ce were incorporated into the catalyst, $Ce_xZr_{1-x}O_2$ solid solution was formed, as confirmed by XRD analyses. TPR results revealed stronger Ni-support interaction in the $Ce_xZr_{1-x}O_2$-modified catalysts than in Ni/SiO_2 one, which can be attributed to an increase of the dispersion of Ni species. All of the Ni/$Ce_xZr_{1-x}O_2$/SiO_2 catalysts exhibited good catalytic activity and stability after 8 h of time on stream at 600 °C . The best catalytic performance in terms of hydrogen selectivity was achieved when the Zr/Ce mass ratio was three.

Keywords: nickel catalyst; ceria; zirconia; promoter; coke; impregnation order

---

1. Introduction

Energy sustainability and reduction of CO_2 emissions will be joined with a decrease in fossil fuel use and the development of green energies. In this sense, hydrogen could be the energy carrier of the future due to its clean and non-polluting nature [1–4]. However, the current hydrogen production routes imply the use of fossil fuel-derived products, like methane, as feedstock and, for this reason, the search of new alternatives for hydrogen production based on renewable resources is essential [5]. In line with this, hydrogen production from ethanol steam reforming is an attractive option, since ethanol can be obtained from a wide variety of biomass feedstocks, and therefore, it can minimize CO_2 emissions. In addition, ethanol has a high H/C atomic ratio, low toxicity and can be easily and safely manipulated and transported [6,7].

The ethanol steam reforming process (ESR) can be represented by the following equation:

$$CH_3CH_2OH + 3H_2O \rightleftarrows 6H_2 + 2CO_2 \quad (1)$$

which involves several steps. The main reaction mechanism comprises dehydrogenation or dehydration routes, which implies the formation of intermediates, like acetylene or ethylene, respectively. Coke formation reactions also participate in the reaction pathway leading to catalyst deactivation [8–10].

Ethanol steam reforming has been investigated using different catalysts [10,11]. In fact, Ni/SiO_2 has been widely used, because it provides good activity and, at the same time, high selectivity to H_2 and CO_x at a relatively low cost [12–19]. This catalytic behavior cannot only be ascribed to the nickel active phase, since the support also affects catalysts activity and product distribution [11,15–18]. In this sense, the use of silica in Ni-Cu-supported catalysts gave better results in comparison to other carrier materials, like alumina and MCM-41 [20]. Despite the good catalytic performance, the literature also describes that Ni/SiO_2 can be deactivated along time on stream, by metal sintering and coke deposition.

Trying to get over this drawback, a number of attempts have been made to prevent deactivation by modifying catalysts through the addition of different elements [16–18]. In this sense, increasing attention has been given to CeO_2 or ZrO_2-CeO_2 mixed oxide, because the oxygen mobility improves catalytic stability through coke gasification [9,11,21–24]. However, CeO_2 and ZrO_2-CeO_2 oxides have a very low surface area to be used as catalytic supports. To increase the textural properties, silica has been incorporated to ZrO_2-CeO_2 [25,26], and the literature also reports how CeO_2 or ZrO_2-CeO_2 were supported on silica to be used in catalytic applications [27,28]. Other researchers describe the addition of ZrO_2 to ceria and silica to increase their thermal resistance and prevent the growth of Ni crystallites [29–31].

Based on the above premises, this work proposes the use of Ce- and Zr-oxides as promoters in the synthesis of Ni/SiO_2 catalyst to reduce catalyst deactivation, allowing nickel particles to accommodate on a porous support in order to avoid or minimize the sinterization of the metallic phase.

2. Results and Discussion

2.1. Ethanol Steam Reforming over Reference Catalysts

Commercial silica, ceria and zirconia with BET surface areas of 276, 64 and 20 m^2/g, respectively, were used as supports of the reference catalysts. The physicochemical properties of the catalyst obtained after the incorporation of nickel into these supports are summarized in Table 1.

Table 1. Physicochemical properties of the reference catalysts.

Catalyst	Ni [a] wt%	S_{BET} m^2/g	Acidity [b] meq-NH_3/g	D^c_{NiO} nm	D^d_{Ni} nm
Ni/S	6.9	263	-	16.4	17.6
Ni/C	6.7	53	-	-	-
Ni/Z	6.8	15	0.275	-	-

[a] ICP-AES; [b] NH_3-temperature programmed desorption (TPD) analysis; [c] calculated from the (200) reflection of NiO in XRD; [d] calculated from the (111) reflection of Ni in XRD.

The actual nickel content measured by ICP-AES was near the nominal loading. Compared to the supports, the BET surface area of the catalysts decreased, although the trend is maintained, Ni/S >Ni/C >Ni/Z. Since the catalyst acidity can influence the products' distribution in the steam reforming reaction, it was measured by NH_3-TPD, verifying that only the Ni/Z catalyst exhibited measurable acidity with a desorption peak around 220 °C , corresponding to 0.275 meq-NH_3/g.

Figure 1 shows the XRD diffractograms of the calcined and reduced catalysts, where peaks corresponding to the carrier materials and those associated with the Ni phase can be observed. For calcined samples, reflections corresponding to the planes (111), (200) and (220) of cubic NiO can be observed at 2θ = 37.3°, 43.3° and 62.9° (JCPDS 78-0643), while peaks attributed to the planes (111) and (200) of metallic Ni appear at 2θ = 44.4° and 51.8° (JCPDS 70-1849) for the reduced catalysts. The intensity of these reflections is hardly noticeable in the case of the Ni/C sample and overlap with ZrO_2 peaks in the Ni/Z sample. Apart from the diffraction of the Ni phase, the pattern of Ni/S shows only one diffuse reflection around 2θ values of 22.5°, typical of certain amorphous materials, while diffraction peaks corresponding to cubic cerium (IV) oxide (JCPDS 89-8436; 2θ = 28.5°, 33.0°, 47.5°, 56.3°, 59.1° and 69.3°) can be clearly observed for Ni/C, and those corresponding to a mixture of monoclinic and tetragonal zirconium (IV) oxide (JCPDS 74-1200 and 80-0784, respectively; main peaks at 2θ = 28.3°, 31.5° and 50.2°) are seen for the Ni/Z catalyst. These analyses were used to calculate the Ni phase crystallites size of the Ni/S sample from the NiO(200) reflection at 2θ = 43.3° and the Ni(111) reflection at 2θ = 44.4° (Table 1). However, accurate crystallite diameters could not be calculated, neither for the Ni/C sample, due to the low intensity of the diffraction lines, nor for the Ni/Z sample, where Ni species peaks overlapped with those of ZrO_2.

The TPR analysis of calcined reference catalysts is shown in Figure 2. The profiles show a main peak between 270 and 350 °C , attributed to the reduction of NiO particles to Ni. In the case of the

Ni/C and Ni/Z samples, the maximum of the reduction peak is placed at lower temperatures, and also, an additional shoulder can be observed, which is attributed to a fraction of the NiO particles strongly interacting with the support. Finally, in the case of the Ni/C sample, another peak arises around 800 °C , due to the partial reduction of Ce^{4+} to Ce^{3+} [21]. TPR analysis of the supports (not shown) demonstrated that, under our experimental conditions, only ceria may give rise to hydrogen consumption with maxima at 800 °C , corresponding to the diffusion-limited partial reduction of bulk CeO_2 particles. The low reduction temperature of Ni/C and Ni/Z catalysts suggests also a weaker metal support interaction in these two catalysts.

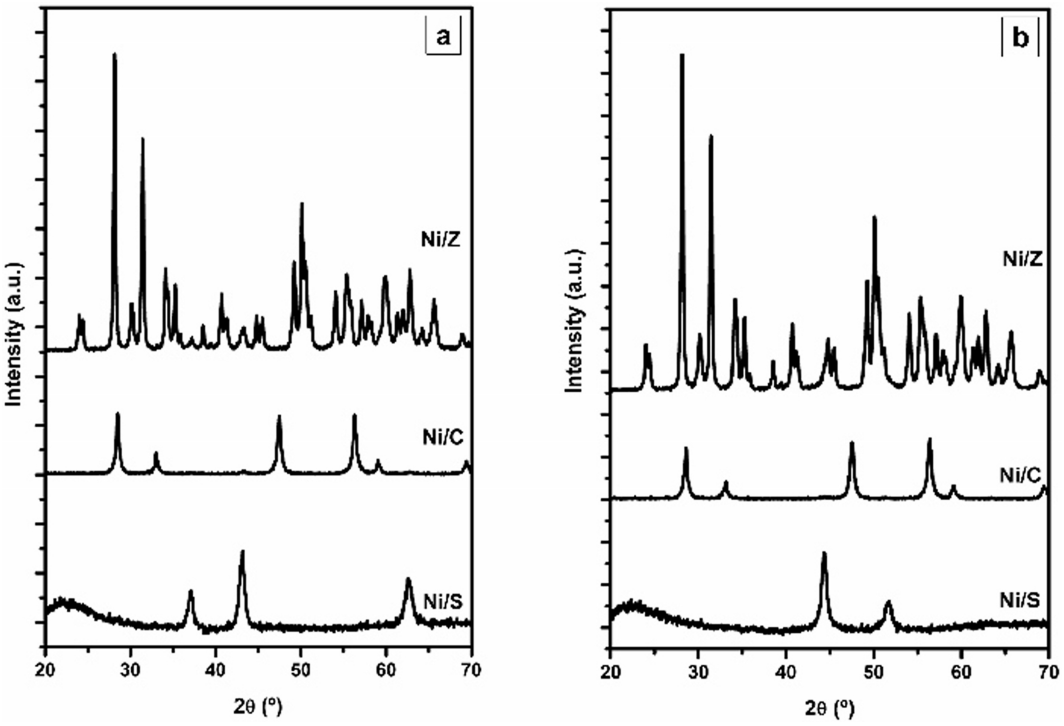

Figure 1. XRD patterns of the calcined (**a**) and reduced (**b**) reference catalysts.

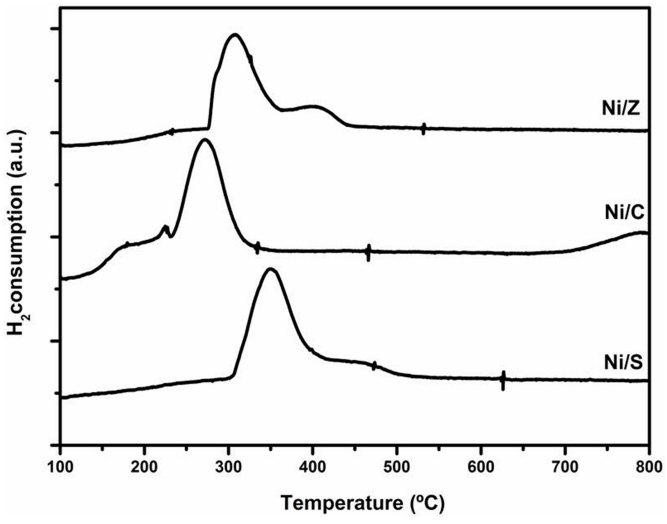

Figure 2. Temperature programmed reduction (TPR) profiles of the calcined reference catalysts.

Table 2 summarizes the results obtained for the ethanol steam reforming reaction after 8 h of time on stream (TOS). While the Ni/C sample kept ethanol conversion above 99%, it decreased to 95.0% and 97.1% after 8 h TOS for the Ni/Z and Ni/S samples, respectively. Regarding intermediate products, acetaldehyde can be detected when using Ni/S and Ni/C, while ethylene is found with the Ni/Z sample due to the presence of acid sites, favoring the ethanol dehydration reaction. Methane selectivity decreases as hydrogen selectivity increases, indicating that methane steam reforming is one of the main steps in the ethanol steam reforming reaction mechanism. Thus, a slight hydrogen selectivity is reached by the Ni/S catalyst in comparison with the rest of samples.

Table 2. Results of ethanol steam reforming obtained with the reference catalysts (atmospheric pressure; T: 600 °C ; weight hourly space velocity; WHSV: 12.7 h^{-1}; $R_{H2O/EtOH}$: 3.7 mol/mol; time on stream (TOS): 8 h).

Catalyst	X_{EtOH}	Selectivity (mol%)					
	mol%	H_2	CO_2	CO	CH_4	C_2H_4	CH_3CHO
Ni/S	97.1	84.2	49.4	31.5	17.4	0	1.7
Ni/C	99.1	82.5	48.0	31.6	19.6	0	0.7
Ni/Z	95.0	80.7	45.3	31.8	20.4	2.4	0

Based on the above results and taking into account that silica is a porous support that could accommodate Ce an Zr oxides, the next study was the modification of Ni/SiO_2 catalysts by Ce or Zr addition.

2.2. Ni/SiO_2 Catalysts Modified by Ce or Zr

2.2.1. Characterization of Ce- or Zr-Modified Silica

For this study, four silica-supported Ni catalysts were prepared and modified by Ce or Zr addition, both before and after the incorporation of Ni. Thus, amorphous silica was used as the support of the Ce and Zr phases, and the XRD patterns of the resulting materials are shown in Figure 3, together with that of the Ni/S sample (described in Section 2.1), where Ce and Zr were later incorporated.

In the case of the CeS sample, the main diffraction peaks characteristic of the planes (111), (200), (220) and (311) of cubic CeO_2 (JCPDS 89-8436) are observed at 2θ = 28.5°, 33.0°, 47.5° and 56.3°. On the other hand, in the diffraction pattern corresponding to the ZrS sample, no clear peaks of Zr species can be seen, although a small broad slope appears around 2θ = 30.2°, which may be attributed to the plane (101) of highly dispersed ZrO_2 in the tetragonal phase (JCPDS 80-0784). This suggests that while Ce trends to aggregate into CeO_2 particles [16], Zr trends to form ZrO_2 crystallites too small to be detected by XRD. This fact agrees with the results published by Sánchez-Sánchez *et al.* [15] with Zr/Al_2O_3, where for Zr loadings up to 6.6 μmol Zr/m^2, Zr ions exists in atomic dispersion. The BET surface area of CeS and ZrS was 267 and 227 m^2/g, respectively, slightly lower in comparison to the silica used as the support, due to the metals' incorporation. Finally, TPR analysis of CeS and ZrS

materials (not shown) evidenced that no detectable hydrogen consumption occurs at the metal loading used in this study (around 10 wt%), in spite of the partial reduction observed for the bulk CeO_2 used as a support in Section 2.1.

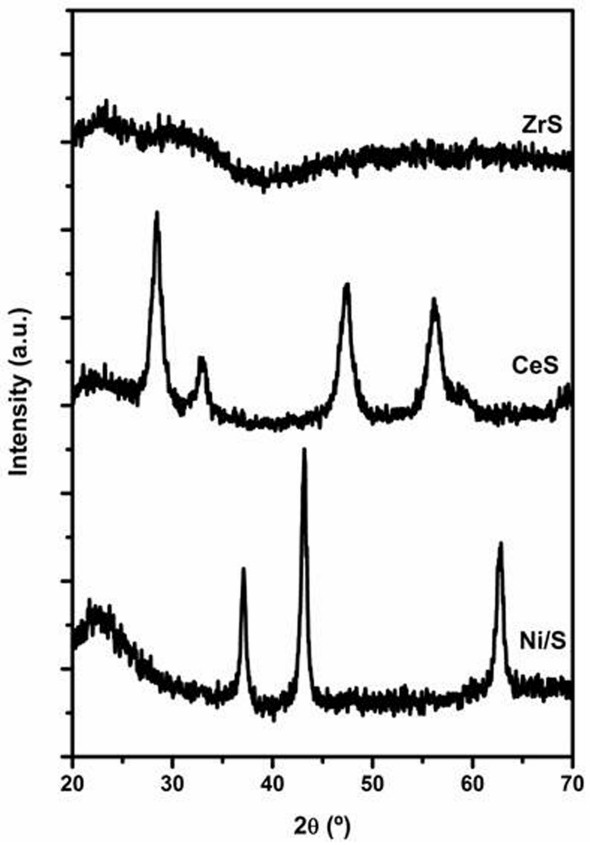

Figure 3. XRD patterns of the Ce- and Zr-modified silica supports.

2.2.2. Characterization of Ce- or Zr-Modified Ni/SiO_2 Catalysts

The physicochemical properties of the prepared Ni catalysts are summarized in Table 3. ICP-AES analysis revealed that silica support was loaded with near the desired amounts of Ni, Ce and Zr. Although the incorporation of a second metal into the previously described materials slightly decreased the value of their textural properties, all of the catalysts exhibited a high BET surface area. The acidity of the materials was measured by NH_3-TPD and is summarized in Table 3. Ce/NiS and Ni/CeS catalysts show negligible acidity, while Zr incorporation into silica support results in the presence of acid sites, which is more pronounced when Zr is incorporated after Ni, probably due to easier accessibility to these acid sites (not covered by Ni).

The XRD spectra of the calcined and reduced catalysts are shown in Figure 4. All of the calcined samples exhibit the peaks characteristic of cubic NiO (JCPDS 78-0643) at 2θ = 37.3°, 43.3° and 62.9°, while the reduced samples show the reflections corresponding to metallic Ni (JCPDS 70-1849) at 2θ = 44.4° and 51.8°. As observed for the corresponding modified support, the main diffraction peaks characteristic of cubic CeO_2 appear in the case of the Ni/CeS and Ce/NiS catalysts, and the broad slope attributed to highly-dispersed ZrO_2 can be seen for the Zr/NiS and Ni/ZrS catalysts. The mean size of the CeO_2 particles, calculated by means of the Scherrer equation, resulted in being higher for the Ce/NiS

sample, which indicates that CeO_2 particles are better dispersed on silica than on Ni/S. Regarding the Ni phase, the mean crystallite sizes are summarized in Table 3. Concerning the calcined samples, both Ce- and Zr-modified catalysts have slightly larger NiO crystallites than the unmodified Ni/S sample (Table 1), mainly when Ni is added to catalyst after Ce or Zr. A similar trend is found for the reduced samples. However, while the Ni phase crystallite size increases after the reduction process for the Ce-modified samples, attributed to the thermal effect, the addition of Zr leads even to a slight reduction of the crystallite size, which may be attributed to higher thermal stability together with lattice contraction from NiO to Ni due to the different molar volumes of these phases.

Table 3. Physicochemical properties of the Ni/SiO_2 catalysts modified by Ce or Zr.

Catalyst	Ni [a] wt%	Ce [a] wt%	Zr [a] wt%	S_{BET} m^2/g	Acidity [b] meq-NH_3/g	D^c_{CeO2} nm	D^d_{NiO} nm	D^e_{Ni} nm
Ce/NiS	6.7	9.7	-	228	-	8.1	19.8	19.9
Zr/NiS	6.7	-	9.4	236	0.144	-	20.0	19.9
Ni/CeS	6.8	9.2	-	247	-	7.0	21.8	23.2
Ni/ZrS	6.9	-	9.9	213	0.133	-	21.6	19.7

[a] ICP-AES measurements; [b] NH_3-TPD analysis; [c] calculated from the (220) reflection of CeO_2 in XRD; [d] calculated from the (200) reflection of NiO in XRD; [e] calculated from the (111) reflection of Ni in XRD.

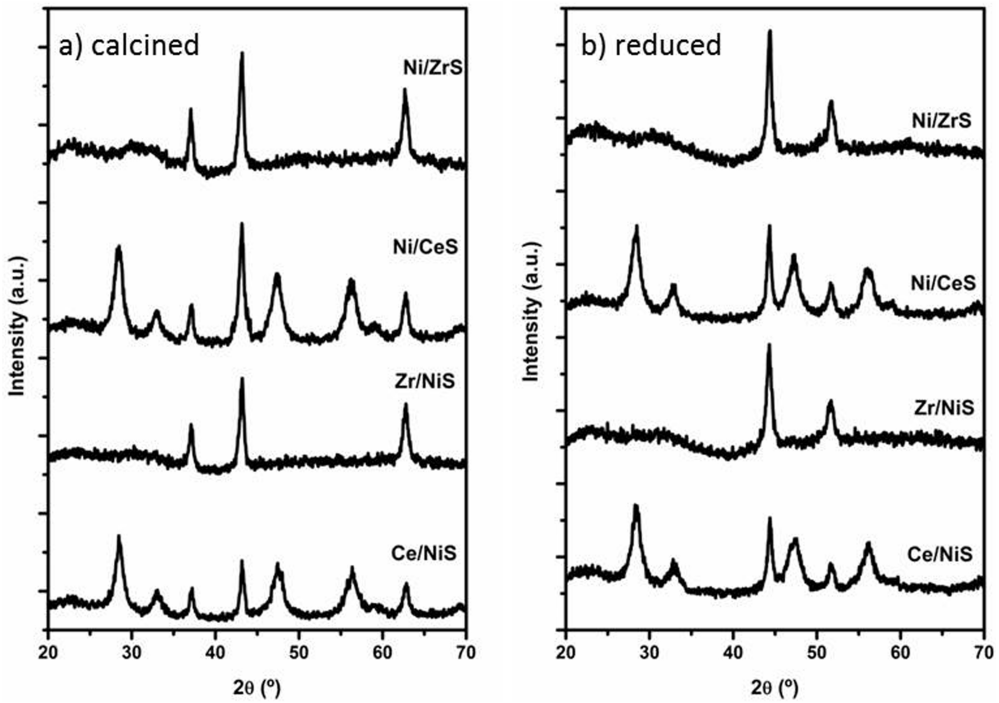

Figure 4. XRD patterns of the Ce- and Zr-modified Ni/SiO_2 catalysts: (**a**) calcined; (**b**) reduced.

The reducibility of these catalysts was determined by H_2-TPR experiments. The profiles shown in Figure 5 exhibit more than one peak attributed to the direct reduction of Ni^{2+} species to Ni, which means the presence of different reducible nickel species depending on the interaction with the support. Quantitative analysis of the TPR profiles revealed total reduction of the Ni^{2+} species for all of the samples. As in the case of the Ni/S sample (Figure 2), the peak at the lower temperature is attributed to the typical reduction of NiO to Ni, which may correspond to relatively large NiO particles, while the shoulder at the higher temperature is ascribed to nickel species in close contact with the support [22,23]. The Ce/NiS sample presents a lower reduction temperature than Ni/S catalyst, indicating the promotion of Ni reducibility by CeO_2 incorporation, an effect typically found for lanthanide elements [16]. On the contrary, reduction of the Zr/NiS sample takes place at higher temperatures, which may indicate an intimate contact between the Ni phase and the promoter due to partial covering of the NiO particles by the highly-dispersed Zr phase added to the Ni/S sample. On the other hand, when Ni was impregnated after Ce or Zr, reduction occurs in a broad temperature range, similarly to the reduction of Ni/S (Figure 2). A shoulder arises in the profile of the Ni/CeS catalyst at slightly lower temperatures than the beginning of the reduction of the Ni/S sample, probably due to the presence of oxygen vacancies in CeO_2, promoting the reduction of NiO [24,32], an effect facilitated by the small dimensions of the CeO_2 crystallites (Table 3). The profile corresponding to the Ni/ZrS sample reaches higher temperatures, probably due to the easier contact between NiO and ZrO_2, which is well dispersed over the support, unlike the CeO_2 particles, as the XRD patterns evidenced. The shift of the Zr-modified catalysts profiles to higher reduction temperatures in comparison to the rest of the samples indicates higher thermal stability and accounts for the decrease in the Ni phase crystallite size after the reduction of the catalyst, as previously observed from the XRD results.

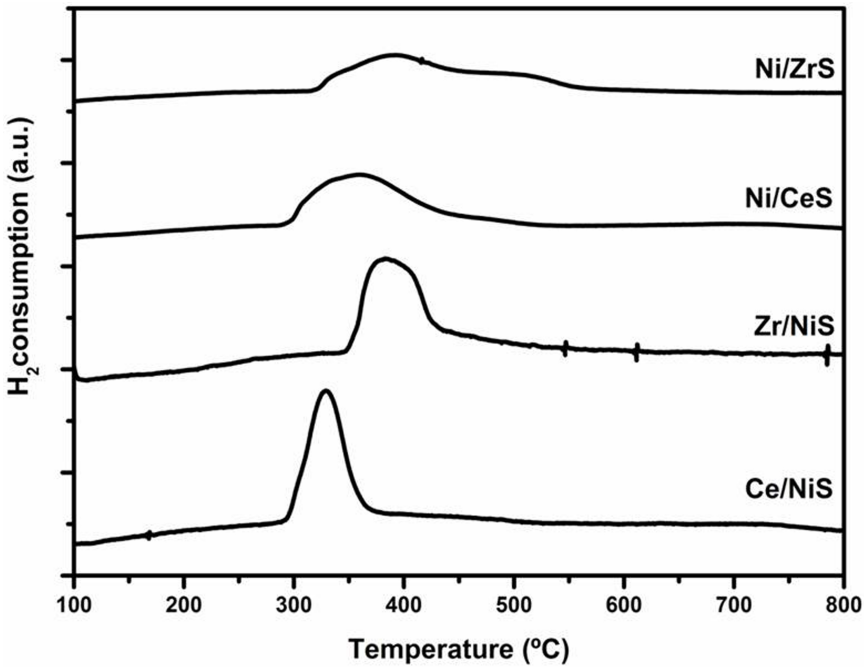

Figure 5. Temperature programmed reduction (TPR) profiles of the calcined Ce- or Zr-modified Ni/SiO_2 catalysts.

2.2.3. Catalytic Results Using Ni/SiO_2 Catalysts Modified by Ce or Zr

The catalytic results obtained by these catalysts after 8 h of TOS on ethanol steam reforming at 600 °C are shown in Table 4. Complete ethanol conversion was maintained over all of the catalysts, except in the case of the Ce/NiS sample, whereas it slightly decreased up to 98.5 after 8 h. On the other hand, hydrogen selectivity is lower for the samples where incorporation of Ni was carried out before the addition of the Ce or Zr, which may be due to some Ni particles covered by the promoters. This effect is more pronounced in the case of the Zr/NiS sample, which reached the lowest hydrogen selectivity, due to the high dispersion of the Zr phase, probably in the form of an overlayer over the Ni particles. However, total ethanol conversion is achieved with this sample, because the acidic nature of this catalyst favors ethanol dehydration to ethylene, as observed from the relatively high C_2H_4 amount obtained among the products. Ethylene selectivity is smaller for the Ni/ZrS sample, as expected from its lower acidity (Table 3). Therefore, regarding the impregnation order of the different elements, the incorporation of Ce or Zr before Ni on SiO_2 leads to lower selectivity to intermediate products and, consequently, higher selectivity towards the main products (H_2 and CO_2). This may be ascribed to the easier accessibility of reactants to the Ni sites. Finally, the CO_2/CO ratio among the gaseous products is increased by the presence of CeO_2, since it favors the water-gas shift reaction [33,34].

Table 4. Results on ethanol steam reforming obtained with the Ni/SiO_2 catalyst modified by Ce or Zr (atmospheric pressure; T: 600 °C ; weight hourly space velocity; WHSV: 12.7 h^{-1}; $R_{H2O/EtOH}$; 3.7 mol/mol; TOS: 8 h).

Catalyst	X_{EtOH}	Selectivity (mol%)						Coke
	mol%	H_2	CO_2	CO	CH_4	C_2H_4	CH_3CHO	g/g_{cat} h
NiS	97.1	84.2	49.4	31.5	17.4	0	1.7	0.369
Ce/NiS	98.5	82.0	49.6	29.9	19.5	0	1.0	0.230
Zr/NiS	100	79.2	43.5	29.1	21.2	6.2	0	0.475
Ni/CeS	100	84.3	56.2	25.1	18.7	0.0	0	0.370
Ni/ZrS	100	88.3	56.5	28.0	12.9	2.6	0	0.518

The results shown in Table 4 indicate that coke formation occurs at a much higher rate on Zr-modified catalysts, because, as explained above, the acid sites joined with the presence of Zr promote ethanol dehydration to ethylene, which acts as a hard precursor for carbon deposition [35]. Although the highest coke amount was found on the Ni/ZrS sample, no loss of activity was observed for this sample, since carbon was deposited in the form of nanofibers (Figure 6). This type of coke does not embed metal particles [36], keeping the metal surface accessible for reactants, which, together with the high surface area of the silica support to accommodate large amounts of coke, has been described to have a minor effect on catalyst deactivation [37,38]. However, high coke formation is not desirable, because it would probably result in reactor plugging. On the other hand, when Ce was added over the Ni/S sample (Ce/NiS), coke formation diminished as a consequence of the enhancement of carbon gasification by

CeO_2 [16,22]. However, in the case of the Ni/CeS sample, this reduction of the coke amount is not observed, due to the higher Ni particles of the catalyst that favors the growth of carbon nanofibers [39,40].

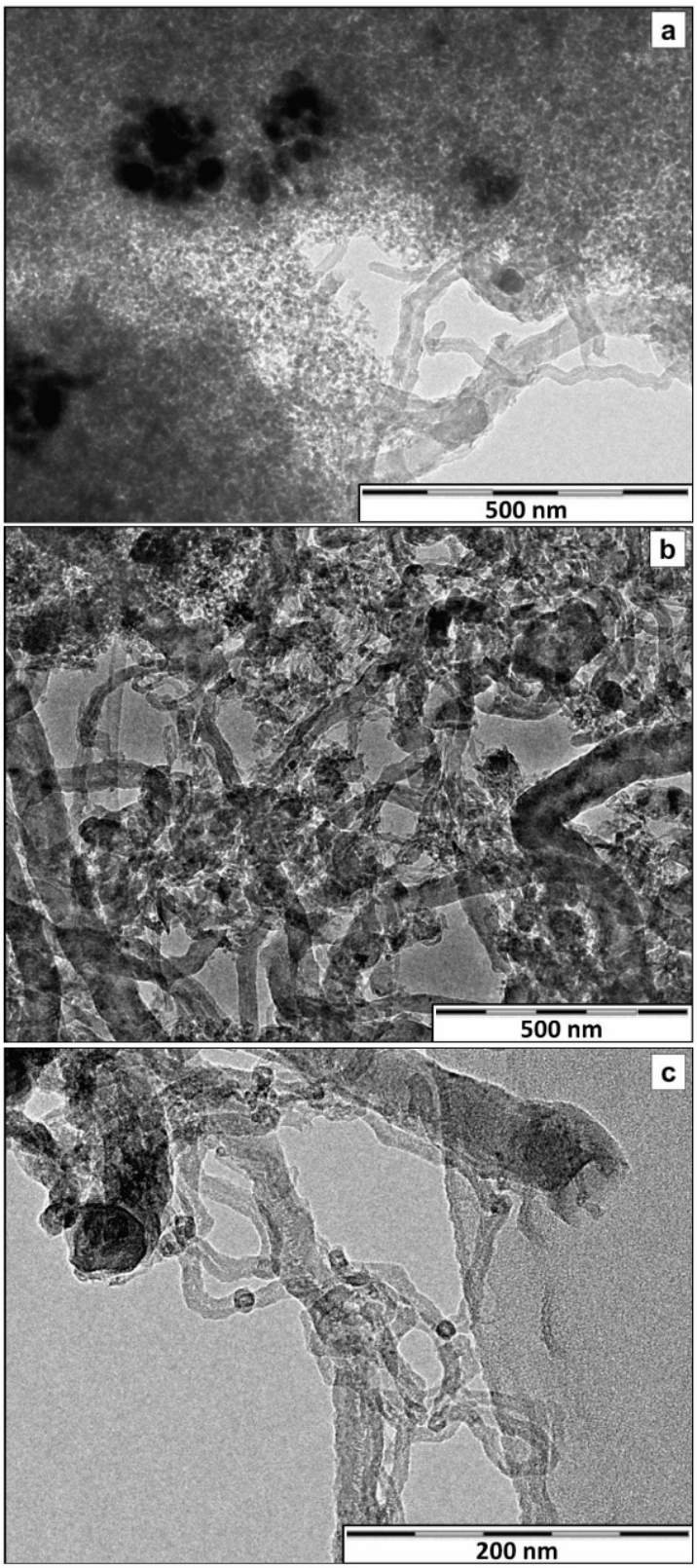

Figure 6. TEM image of coke formed on catalysts after being used for ethanol steam reforming for 8 h: (**a**) Ni/S; (**b**) Ce/NiS; (**c**) Ni/ZrS.

Consequently, taking into account that the highest hydrogen selectivity was reached with the Ni/ZrS catalyst at complete ethanol conversion and Ce/NiS led to a lesser amount of carbon deposited on the catalyst, the next study consisted of the modification of Ni/SiO_2 catalysts by both Ce and Zr incorporation before the Ni phase.

2.3. Ni/$Ce_xZr_{1-x}O_2$/SiO_2 Catalysts: The Effect of the Zr/Ce Ratio

2.3.1. Characterization of the $Ni/Ce_xZr_{1-x}O_2/SiO_2$ Catalysts

For this study, three Ni catalysts supported on Ce- and Zr-modified silica were prepared with Zr/Ce mass ratios of 1/3, 1 and 3. Their physicochemical properties are shown in Table 5, where it can be observed that there is a good agreement between the metal contents determined by ICP-AES and the theoretical values. All of the catalysts show a high surface area in comparison to the values corresponding to the Ni/C and Ni/Z catalysts (Table 1), as expected from the use of silica as a support. However, they exhibit lower BET surface areas than the Ni/S sample, with a slight decreasing trend as the Zr content increases (Table 3). As expected, the acidity of the materials measured by NH_3-TPD increased with the Zr loading, the Ni/ZrS catalyst having the highest number of acid sites.

Table 5. Physicochemical properties of the $Ni/Ce_xZr_{1-x}O_2/SiO_2$ catalysts.

Catalyst	Ni [a] wt%	Ce [a] wt%	Zr [a] wt%	S_{BET} m^2/g	Acidity [b] meq_{NH3}/g	D^c_{CeO2} nm	D^d_{NiO} nm	D^e_{Ni} nm
Ni/CeZrS-1/3	6.8	6.0	2.3	243	0.062	6.3	19.1	19.7
Ni/CeZrS-1	7.0	4.2	4.5	242	0.077	5.0	18.1	16.6
Ni/CeZrS-3	6.6	2.4	6.6	238	0.088	3.4	17.6	15.7

[a] ICP-AES measurements; [b] NH_3-TPD analysis; [c] calculated from the (220) reflection of CeO_2 in XRD; [d] calculated from the (200) reflection of NiO in XRD; [e] calculated from the (111) reflection of Ni in XRD.

The XRD spectra of the calcined and reduced catalysts are shown in Figure 7, where samples containing both Ce and Zr have a pattern similar to that of Ni/CeS sample (Figure 4), but CeO_2 peaks become less intense and shift to higher 2θ values with increasing Zr loading. This fact has been ascribed to the formation of a $Ce_xZr_{1-x}O_2$ solid solution, where the unit cell parameter changes with the Zr/Ce ratio [21,23,26]. The size of the CeO_2 crystallites on calcined catalysts were calculated from the width of the (220) characteristic peak. The values displayed in Table 5 show that crystallites found on these catalysts are smaller than those reported for unsupported $Ce_xZr_{1-x}O_2$ [21], which evidences that the relatively high surface area of SiO_2 enhances their dispersion, and their sizes become smaller as the Zr/Ce ratio increases. Only a slight increment of these particles sizes ($\approx$ 0.1–0.3 nm) was detected after reduction treatment.

Additionally, the peaks characteristic of cubic NiO (JCPDS 78-0643) and those corresponding to metallic Ni (JCPDS 70-1849) can be observed for the calcined and reduced samples, respectively.

Concerning the calcined samples, the mean NiO crystallites sizes, calculated by applying the Scherrer equation to the broadening of the (200), are summarized in Table 5. The NiO crystallite size decreases as the Zr content is increased, which has been previously reported for unsupported $Ce_xZr_{1-x}O_2$ catalysts [15,20]. In the case of the reduced samples, the Ni crystallite sizes follow a similar trend. It is noticeable that Ni crystallites of the reduced Ni/CeZrS-1 and Ni/CeZrS-3 catalysts are smaller than the Ni particles of the corresponding calcined samples and even smaller than Ni crystallites of Ni/S catalyst, Ni/CeZrS-3 being the catalyst with the smallest Ni crystallites.

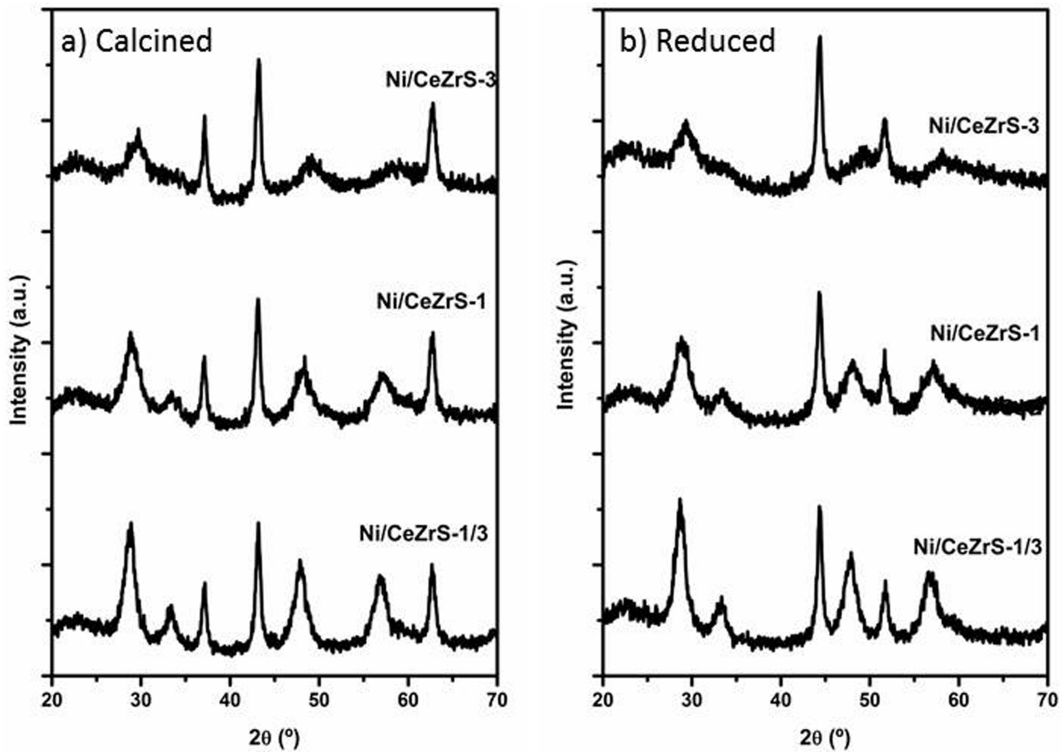

Figure 7. XRD patterns of the Ni/$Ce_xZr_{1-x}O_2$/SiO_2 catalysts: (**a**) calcined; (**b**) reduced.

The reducibility of these catalysts was determined by H_2-TPR experiments, and the corresponding profiles shown in Figure 8 evidenced a similarity with those of the Ni/CeS and Ni/ZrS samples. These profiles have a peak at a lower temperature due to the reduction of NiO particles and a shoulder at a higher temperature ascribed to the reduction of nickel species in close contact with the support. Quantitative analysis of the TPR profiles revealed total reduction of the Ni^{2+} species for all of the samples. By increasing the ZrO_2 content, the reduction profiles slightly shift towards higher temperatures, and this peak area increases while the area under the low temperature zone decreases. This fact indicates a stronger interaction of Ni^{2+} species with the support as ZrO_2 loading increases [15,18,19], which accounts for the hindered sintering of the Ni phase when Zr loading increases, as observed from the difference between the mean size of the nickel phase crystallites before and after reduction (see Table 5). The decrease of the $Ce_xZr_{1-x}O_2$ particle size as the Zr loading increases would make it possible for a higher contact between this phase and the NiO, which results in higher metal-support interaction [16].

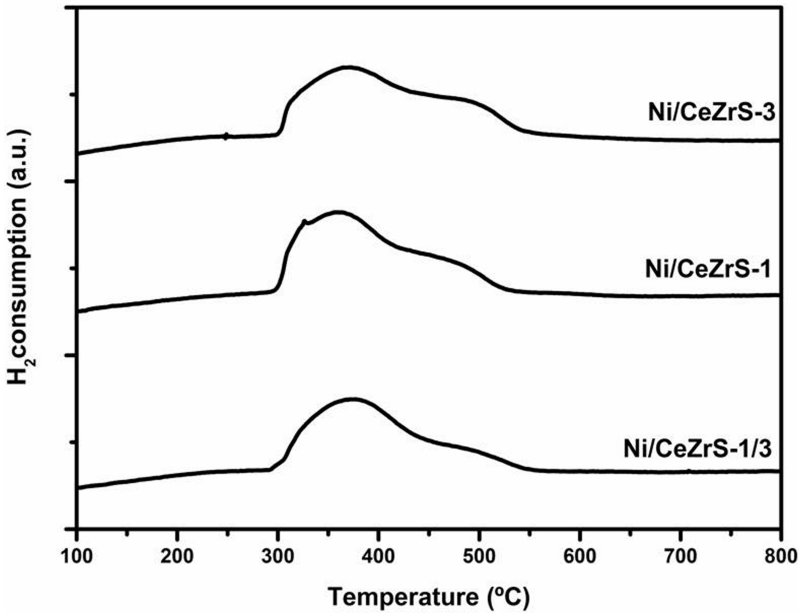

Figure 8. TPR profiles of the calcined Ni/$Ce_xZr_{1-x}O_2$/SiO_2 catalysts.

2.3.2. Catalytic Results Using the Ni/$Ce_xZr_{1-x}O_2$/SiO_2 Catalysts

These catalysts were tested at 600 °C in the ethanol steam reforming, and the obtained results are shown in Table 6. All of the catalysts showed complete ethanol conversion after 8 h of TOS. On the other hand, it can be observed how product selectivity depends on the Zr/Ce ratio. The only H-containing intermediate compound found among the reaction products was methane, while neither ethylene nor acetaldehyde could be detected. Besides, as the Zr/Ce ratio is increased, selectivity towards CH_4 decreases, and thus, hydrogen selectivity increases. This may be attributed to both a decrease of Ni crystallite size and an increase of thermal stability when the Zr content increases, as determined by XRD and TPR (Table 5 and Figure 8). Regarding the CO_2/CO ratio, it is higher for Ni/$Ce_xZr_{1-x}O_2$/SiO_2 catalysts than for the Ni/S sample and increases with the Zr/Ce ratio. An enhanced oxygen storage capacity due to the formation of the $Ce_xZr_{1-x}O_2$ solid solution has been reported to favor the water-gas shift reaction [23,26].

Table 6. Results on ethanol steam reforming obtained with the Ni/$Ce_xZr_{1-x}O_2$/SiO_2 catalysts (atmospheric pressure; T: 600 °C ; weight hourly space velocity (WHSV): 12.7 h^{-1}; $R_{H2O/EtOH}$: 3.7 mol/mol; TOS: 8 h).

Catalyst	X_{EtOH}	Selectivity (mol%)						Coke
	mol%	H_2	CO_2	CO	CH_4	C_2H_4	CH_3CHO	g/g_{cat} h
Ni/CeZrS-1/3	100	84.6	52.4	29.6	18.0	0	0	0.500
Ni/CeZrS-1	100	85.6	54.0	29.0	17.0	0	0	0.443
Ni/CeZrS-3	100	85.8	54.3	28.9	16.8	0	0	0.308

Finally, Table 6 compares catalysts in terms of coke formation, which decreases as the Zr/Ce mass ratio in the catalyst increases. However, since ceria and zirconia improve oxygen mobility [32,41,42], favoring carbon gasification, coke deposition on promoted catalysts decreased by increasing Zr content in the $Ce_xZr_{1-x}O_2$ solution, which agrees with the smaller size of NiO and Ni crystallites found in samples with a higher Zr content.

3. Experimental Section

3.1. Catalysts Preparation

A series of catalysts were prepared to study the effect of the addition of Ce and Zr to Ni/SiO_2 catalyst (Ni: 7 wt%). The modified catalysts contain a total loading of Ce and Zr of 10 wt% and Ce/Zr mass ratios of 0, 1/3, 1, 3 and ∞. Moreover, the order of the Ce or Zr incorporation with SiO_2, before or after Ni addition, was also studied. The addition of metals was accomplished by incipient wetness impregnation of amorphous silica (Ineos, Warrington, UK) with aqueous solutions of the metal precursors: $Ni(NO_3)_2{\cdot}6H_2O$ (Scharlab, Sentmenat, Barcelona, Spain), $Ce(NO_3)_3{\cdot}6H_2O$ (Scharlab, Sentmenat, Barcelona, Spain) and $ZrO(NO_3)_2{\cdot}6H_2O$ (Sigma–Aldrich, St. Louis, MO, USA). After the incorporation of each metal (Ni, Zr or Ce), the solid sample was air-dried overnight and further calcined at 500 °C for 5 h with a heating rate of 1.8 °C /min. Afterwards, the addition of the other metal, if needed, was carried out by following the same procedure. Ni/SiO_2, Ni/CeO_2 and Ni/ZrO_2 were prepared as reference materials by impregnation of Ni over commercial silica (Ineos, Warrington, UK), ceria (Riedel-de-Haën, Hanover, Germany) and zirconia (Sigma–Aldrich, St. Louis, MO, USA). Catalyst are denoted as A/BY-*x*, where A/B are the metals added to the support (A, secondly, and B, firstly added), Y is the support (S: silica, C: ceria and Z: zirconia), and *x* is the Zr/Ce mass ratio in the final sample.

3.2. Catalysts Characterization

X-ray powder diffraction (XRD) analysis was used to find out the crystalline phases and calculate mean crystallite size in the calcined and reduced catalysts. Measurements were carried out on a Phillips (Eindhoven, The Netherlands) X'Pert PRO diffractometer using Cu Kα radiation. The patterns were recorded with a 2θ increment step of 0.020° and a collection time of 2 s. Mean metallic crystallite diameters were calculated by applying the Scherrer equation.

The inductively-coupled plasma atomic emission spectroscopy (ICP-AES) technique was used to determine the total Ce, Zr and Ni content in the catalysts using a Varian (Palo Alto, CA, USA) VISTA-PRO AX CCD-Simultaneous ICP-AES spectrophotometer. Samples were previously dissolved with an acidic solution (HF and H_2SO_4).

Textural properties of the materials were calculated by nitrogen adsorption-desorption at 77 K in a Micromeritics (Norcross, GA, USA) TRISTAR 2050 sorptometer. Samples were first outgassed under vacuum at 200 °C for 4 h. Surface areas were determined using the BET method.

Acid properties of the catalysts and supports were obtained by ammonia temperature programmed desorption analysis (NH_3-TPD) in a Micromeritics (Norcross, GA, USA) Autochem 2910 equipment.

Samples were previously outgassed under a He flow (50 NmL/min) at 560 °C for 30 min. After saturation of the sample with ammonia and removal of the physisorbed fraction by flowing He at 180 °C , NH_3 was desorbed from the sample by increasing the temperature up to 550 °C with a heating rate of 15 °C /min, keeping this temperature constant for 30 min.

The reducibility of supported metals was determined by hydrogen temperature programmed reduction analysis (H_2-TPR). Catalysts were analyzed with the same apparatus described for NH_3-TPD. Catalysts were previously degasified in flowing argon (35 mL/min) for 30 min at 110 °C with a heating rate of 15 °C /min. Afterwards, the H_2-TPR profile was obtained by flowing 10% H_2 in Ar (35 NmL/min) from 25 °C to 800 °C with a heating rate of 5 °C /min.

The morphology of catalyst particles and metal crystallites was analyzed by transmission electron microscopy (TEM). Samples were prepared by dispersion of the powdered material in acetone and following deposition on a copper grid with carbon support. Micrographs were attained on a Phillips (Eindhoven, The Netherlands) TECNAI 20 equipped with a LaB_6 filament and an accelerating voltage of 200 kV.

Carbon deposited on the used catalysts was evaluated by thermogravimetric analysis (TG). TG measurements were carried out on a TA instruments (New Castle, DE, USA) SDT 2960 thermobalance using an air flow of 100 mL/min and a heating rate of 5 °C /min up to 700 °C .

3.3. Catalytic Test

Catalysts activity and selectivity were measured in the ethanol steam reforming reaction on a MICRO ACTIVITY-PRO unit, as described elsewhere [19]. The catalyst was placed into the reactor and *in situ* reduced under flowing pure hydrogen (30 NmL/min) for 4.5 h at 550 °C with a heating rate of 2 °C /min. After activation, the catalytic tests were carried out at atmospheric pressure and 600 °C . A liquid water/ethanol (3.7 molar ratio) stream (0.075 mL/min) was fed into the system, vaporized at 150 °C and further diluted by N_2 (30 NmL/min). Weight hourly space velocity (WHSV), defined as the water-ethanol mass flow rate related to the mass of the catalyst, was fixed at 12.7 h^{-1}. The composition of the output gas stream was determined online by a gas chromatograph, Varian (Palo Alto, CA, USA) CP-3380, equipped with Hayesep Q and Molecular Sieve 13X columns, a thermal conductivity detector and using He as the carrier and reference gas. Condensable vapors (ethanol, water and acetaldehyde) were retained in a condenser and analyzed by chromatography.

4. Conclusions

Ethanol has been successfully converted into hydrogen though steam reforming over Ni catalysts supported on SiO_2, CeO_2, ZrO_2 and Ce- and/or Zr-modified SiO_2 with different Zr/Ce mass ratios. The Ni/SiO_2 catalyst led to higher hydrogen selectivity than Ni/CeO_2 and Ni/ZrO_2, but it could not maintain complete ethanol conversion. Incorporation of Zr to Ni/SiO_2 increased the Ni-support interaction, leading to complete ethanol conversion along time and higher hydrogen selectivity. However, large amounts of coke were formed as a consequence of ethylene formation induced by acid sites found on Zr-modified catalysts. On the contrary, lower coke formation was observed when Ce was incorporated into Ni/SiO_2, which can be ascribed to the presence of oxygen vacancies in CeO_2 promoting coke

gasification. Concerning the impregnation order, the incorporation of Ce and Zr prior to nickel on the silica support led to steam reforming catalysts with better performance. When both Zr and Ce were incorporated into Ni/SiO_2, a $Ce_xZr_{1-x}O_2$ solid solution was formed, increasing the Ni-support interaction and producing smaller Ni crystallites as the Zr/Ce mass ratio increased. As a result, complete ethanol conversion and hydrogen selectivity above 84 mol% were reached with the $Ni/Ce_xZr_{1-x}O_2/SiO_2$ catalysts. Concretely, using a Zr/Ce mass ratio of three, a trade-off between high selectivity to the main products, relatively low coke deposition and high thermal stability was achieved.

Acknowledgments

The authors acknowledge the financial support from the Ministerio de Economía y Competitividad through the project "Hydrogen and liquid fuels production from microalgae by thermochemical proceses" (Ref: CTQ2013-44447-R), and from the Comunidad de Madrid through the project "Residuals to Energy part 2" project (Ref: P2013/MAE-2882).

Author Contributions

This work was conceived by Jose Antonio Calles and Alicia Carrero. Montaña Lindo did the experimental work, assisted by Arturo Javier Vizcaíno who also draft the first version of manuscript. Furthermore, Arturo Javier Vizcaíno, Jose Antonio Calles and Alicia Carrero wrote and revised the final version of paper.

Conflicts of Interest

The authors declare no conflict of interest.

References

1. Züttel, A.; Remhof, A.; Borgschulte, A.; Friedrichs, O. Hydrogen: the future energy carrier. *Phil. Trans. R. Soc. A* **2012**, *368*, 3329–3342.
2. Guo, L.J.; Zhao, L.; Jing, D.W.; Lu, Y.J.; Yang, Y.J.; Bai, B.F.; Zhang, X.M.; Ma, L.J.; Wu, X.M. Solar hydrogen production and its development in China. *Energy* **2009**, *34*, 1073–1090.
3. Olateju, B.; Kumar, A. Hydrogen production from wind energy in Western Canada for upgrading bitumen from oil sands. *Energy* **2011**, *36*, 6326–6339.
4. Zahedi, A. Hydrogen as storage option for intermittent renewable technologies such as solar and wind. In Proceedings of the 2006 Australasian Universities Power Engineering Conference (AUPEC'06), Melbourne, Australia, 10–13 December 2006.
5. Goltsova, V.A.; Veziroglu, T.N.; Goltsova, L.F. Hydrogen civilization of the future—A new conception of the IAHE. *Int. J. Hydrogen Energy* **2006**, *31*, 153–159.
6. Grzegorczyk, W.; Denis, A.; Gac, W.; Ioannides, T.; Machocki, A. Hydrogen Formation via Steam Reforming of Ethanol Over Cu/ZnO Catalyst Modified with Nickel, Cobalt and Manganese. *Catal. Lett.* **2009**, *128*, 443–448.

7. Vizcaíno, A.J.; Carrero, A.; Calles, J.A. Hydrogen Production from Bioethanol. In *Hydrogen Production: Prospects and Processes*; Nova Science Publishers, Inc.: New York, NY, USA, 2012; pp. 247–294
8. Papadopoulou, E.; Delimaris, D.; Denis, A.; Machocki, A.; Ioannides, T. Alcohol reforming on cobalt-based catalysts prepared from organic salt precursors. *Int. J. Hydrogen Energy* **2007**, *37*, 16375–16381.
9. Navarro, R.M.; Peña, M.A.; Fierro, J.L.G. Hydrogen production reactions from crbon feedstocks: Fossil fuels and biomass. *Chem. Rev.* **2007**, *107*, 3952–3991.
10. Ni, M.; Leung, D.Y.C.; Leung, M.K.H. A review on reforming bio-ethanol for hydrogen production. *Int. J. Hydrogen Energy* **2007**, *32*, 3238–3247.
11. Auprête, F.; Descorme, C.; Duprez, D. Bio-ethanol catalytic steam reforming over supported metal catalysts. *Catal. Commun.* **2002**, *3*, 263–267.
12. Comas, J.; Mariño, F.; Laborde, M.; Amadeo, N. Bio-ethanol steam reforming on Ni/Al_2O_3 catalyst. *Chem. Eng. J.* **2004**, *98*, 61–68.
13. Fatsikostas, A.N.; Verykios, X.E. Reaction network of steam reforming of ethanol over Ni–based catalysts. *J. Catal.* **2004**, *225*, 439–452.
14. Frusteri, F.; Freni, S.; Spadaro, L.; Chiodo, V.; Bonura, G.; Donato, S.; Cavallaro, S. H_2 production for MC fuel cell by steam reforming of ethanol over MgO supported Pd, Rh, Ni and Co catalysts. *Catal. Commun.* **2004**, *5*, 611–615.
15. Sánchez-Sánchez, M.C.; Navarro, R.M.; Fierro, J.L.G. Ethanol steam reforming over Ni/M_xO_y-Al_2O_3 (M = Ce, La, Zr and Mg) catalysts: Influence of support on the hydrogen production. *Int. J. Hydrogen Energy* **2007**, *32*, 1462–1471.
16. Calles, J.A.; Carrero, A.; Vizcaíno, A.J. Ce and La modification of mesoporous Cu-Ni/SBA-15 catalysts for hydrogen production through ethanol steam reforming. *Micropor. Mesopor. Mater.* **2009**, *119*, 200–207.
17. Vizcaíno, A.J.; Carrero, A.; Calles, J.A. Ethanol steam reforming on Mg- and Ca-modified Cu-Ni/SBA-15 catalysts. *Catal. Today* **2009**, *146*, 63–70.
18. Lindo, M.; Vizcaíno, A.J.; Calles, J.A.; Carrero, A. Ethanol steam reforming on Ni/Al-SBA-15 catalysts: Effect of the aluminium content. *Int. J. Hydrogen Energy* **2010**, *35*, 5895–5901.
19. Vizcaíno, A.J.; Lindo, M.; Carrero, A.; Calles, J.A. Hydrogen production by steam reforming of ethanol using Ni catalysts based on ternary mixed oxides prepared by coprecipitation. *Int. J. Hydrogen Energy* **2012**, *37*, 1985–1992.
20. Vizcaíno, A.J.; Carrero, A.; Calles, J.A. Hydrogen production by ethanol steam reforming over Cu-Ni supported catalysts. *Int. J. Hydrogen Energy* **2007**, *32*, 1450-1461.
21. Biswas, P.; Kunzru, D. Steam reforming of ethanol for production of hydrogen over Ni/CeO_2-ZrO_2 catalysts: Effect of support and metal loading. *Int. J. Hydrogen Energy* **2007**, *32*, 969–980.
22. Biswas P.; Kunzru, D. Oxidative steam reforming of ethanol over Ni/CeO_2-ZrO_2 catalyst. *Chem. Eng. J.*, **2008**, *136*, 41–49.
23. Youn, M.H.; Seo, J.G.; Cho, K.M.; Park, S.; Park, D.R.; Jung, J.C.; Song, I.K., Hydrogen production by auto-thermal reforming of ethanol over nickel catalysts supported on Ce-modified mesoporous zirconia: Effect of Ce/Zr molar ratio. *Int. J. Hydrogen Energy* **2008**, *33*, 5052–5059.

24. Wan, H.; Li, X.; Ji, S.; Huang, B.; Wang, K.; Li, C. Effect of Ni loading and $Ce_xZr_{1-x}O_2$ promoter on Ni-based SBA-15 catalysts for steam reforming of methane. *J. Nat. Gas Chem.* **2007**, *16*, 139–147.
25. Rocchini, E.; Vicario, M.; Llorca, J.; Leitenburg, C.; Dolcetti, G.; Trovarelli, A. Reduction and oxygen storage behavior of noble metals supported on silica-doped ceria. *J. Catal.* **2002**, *211*, 407–421.
26. Raju, V.; Jaenicke, S.; Chuah, G.K. Effect of hydrothermal treatment and silica on thermal stability and oxygen storage capacity of ceria-zirconia. *Appl. Catal. B* **2009**, *191*, 92–100.
27. Reddy, B.M.; Thrimurthulu, G.; Saikia, P.; Bharali, P. Silica supported ceria and ceria-zirconia nanocomposite oxides for selective dehydration of 4-methylpentan-2-ol. *J. Mol. Catal. A* **2007**, *275*, 167–173.
28. Reddy, B.M.; Saikia, P.; Bharali, P.; Katta, L.; Thrimurthulu, G. Highly dispersed ceria and ceria-zirconia nanocomposites over silica surface for catalytic applications. *Catal. Today* **2009**, *141*, 109–114.
29. Takahashi, R.; Sato, S.; Sodesawa, T.; Yoshida, M.; Tomiyama, S. Addition of zirconia in Ni/SiO_2 catalyst for improvement of steam resistance. *Appl. Catal. A* **2004**, *273*, 211–215.
30. Seo, J.G.; Youn, M.H.; Song, I.K. Effect of SiO_2-ZrO_2 supports prepared by a grafting method on hydrogen production by steam reforming of liquefied natural gas over Ni/SiO_2-ZrO_2 catalysts. *J. Power Sources* **2007**, *168*, 251–257.
31. Roh, H.S.; Potdar, H.S.; Jun, K.W. Carbon dioxide reforming of methane over co-precipitated Ni-CeO_2, Ni-ZrO_2 and Ni-Ce-ZrO_2 catalysts. *Catal. Today* **2004**, *93–95*, 39–44.
32. Trovarelli, A. *Catalysis by Ceria and Related Materials*; Imperial College Press: London, UK, 2002.
33. Djinovic, P.; Batista, J.; Pintar, A. WGS reaction over nanostructures CuO-CeO_2 catalysts prepared by hard template method: Characterization, activity and deactivation. *Catal. Today* **2009**, *147*, 191–197.
34. Andreeva, D.; Ivanov, I.; Ilieva, L.; Sobczak, J.W.; Avdeev, G.; Tabakova, T. Nanosized gold catalysts supported on ceria and ceria-alumina for WGS reaction: Influence of preparation method. *Appl. Catal. A* **2007**, *333*, 153–160.
35. Trim, D.L. Coke formation and minimisation during steam reforming reactions. *Catal. Today* **1997**, *37*, 233–238.
36. Carrero, A.; Calles, J.A.; Vizcaíno, A.J. Hydrogen production by ethanol steam reforming over Cu-Ni/SBA-15 supported catalysts prepared by direct synthesis and impregnation.*Appl. Catal. A* **2007**, *327*, 82–94.
37. Wang, S.; Lu, G.Q. Reforming of methane with carbon dioxide over Ni/Al_2O_2 catalysts: Effect of nickel precursor. *Appl. Catal.* **1998**, *69*, 271–280.
38. Juan-Juan, J.; Román-Martínez, M.C.; Illán-Gómez, M.J. Effect of potassium content in the activity of K-promoted Ni/Al_2O_2 catalysts for the dry reforming of methane. *Appl. Catal.* **2006**, *301*, 9–15.
39. Carrero, A.; Calles, J.A.; Vizcaíno, A.J. Effect of Mg and Ca addition on coke deposition over Cu-Ni/SiO_2 catalysts for ethanol steam reforming. *Chem. Eng. J.* **2010**, *163*, 395–402.

40. Helveg, S.; Sehested, J.; Rostrup-Nielsen, J.R. Whisker carbon in perspective. *Catal. Today* **2011**, *178*, 42–46.
41. Natesakhawat, S.; Watson, R.B.; Wang, X.; Ozkan, U.S. Deactivation characteristics of lanthanide-promoted sol-gel Ni/Al_2O_2 catalysts in propane steam reforming. *J. Catal.* **2005**, *234*, 496–508.
42. Bellido, J.D.A.; Assaf, E.M. Nickel catalysts supported on ZrO_2, Y_2O_3-stabilized ZrO_2 and CaO-stabilized ZrO_2 for the steam reforming of ethanol: Effect of the support and nickel load. *J. Power Sources* **2008**, *177*, 24–32.